Published in final edited form as:
Chem Biol. 2012 February 24; 19(2): 287–296. doi:10.1016/j.chembiol.2011.11.009.

ATP-independent control of autotransporter virulence protein transport via the folding properties of the secreted protein

Jonathan P. Renn[†,‡], **Mirco Junker**[†,‡], **Richard N. Besingi**, **Esther Braselmann**, and **Patricia L. Clark**[Δ,*]

Department of Chemistry & Biochemistry, University of Notre Dame, Notre Dame IN 46556-5670 USA

[Δ]Eck Institute for Global Health, University of Notre Dame, Notre Dame IN 46556-5670 USA

Summary

Autotransporter (AT) proteins are the largest class of extracellular virulence proteins secreted from Gram-negative bacteria. The mechanism by which AT proteins cross the bacterial outer membrane (OM), in the absence of ATP or another external energy source, is unknown. Here we demonstrate a linear correlation between localized regions of stability ($\Delta G_{folding}$) in the mature virulence protein (the AT "passenger") and OM secretion efficiency. Destabilizing the C-terminal β-helical domain of a passenger reduced secretion efficiency. In contrast, destabilizing the globular N-terminal domain of a passenger produced a linearly correlated increase in secretion efficiency. Thus, C-terminal passenger stability facilitates OM secretion, whereas N-terminal stability hinders it. The contributions of regional passenger stability to OM secretion demonstrate a crucial role for the passenger itself in directing its secretion, suggesting a novel type of ATP-independent, folding-driven transporter.

Keywords

protein folding; Brownian ratchet; Type Va secretion; autotransporter; Gram-negative pathogen

Introduction

Gram-negative bacterial infections lead to diverse human diseases, including bacterial meningitis, dysentery, whooping cough, peptic ulcers, pneumonia, peritonitis, and cholera. Like all pathogenic bacteria, Gram-negative pathogens must secrete a wide variety of proteins to the outer bacterial surface, where these proteins perform crucial functions for the attachment to, recruitment of essential nutrients from, and invasion and disabling of

[*]To whom correspondence should be addressed: pclark1@nd.edu, (574)631-8353 [phone], (574)631-6652 [fax].
[†]These authors contributed equally to this work.
[‡]Current addresses: JPR: Department of Molecular Biosciences, Northwestern University, Evanston, IL 60208 MJ: Department of Cell Biology, Harvard Medical School, Boston, MA 02115

Author Contributions

J.P.R. and M.J. contributed equally to the laboratory work and data analysis. R.N.B. performed and analyzed the fluorescence microscopy experiments. E. B. contributed to the laboratory work and data analysis. P.L.C. conceived the project, analyzed the data, and wrote the paper.

mammalian host cells. Gram-negative bacteria use at least seven distinct mechanisms for secretion of proteins across the outer membrane (OM), but the most common OM secretion mechanism is autotransporter (AT; also known as Type Va) secretion. The AT secretion mechanism was originally named to reflect the apparently independent OM secretion behavior of AT proteins: when placed in a heterologous Gram-negative host, most AT genes are readily expressed and the encoded protein transported to the extracellular milieu, suggesting minimal reliance on host-specific factors to facilitate OM transport (Loveless and Saier, 1997). Each AT is synthesized as a tripartite pre-protein containing an N-terminal signal sequence that directs secretion across the inner membrane, a central "passenger" that represents the mature extracellular virulence protein, and a C-terminal OM porin (the "β-domain") that is essential for OM transport. AT passengers have highly diverse sequences, lengths, and functions, but almost all are predicted to contain β-helical structure (Kajava et al., 2001; Junker et al., 2006). While it was originally proposed that an AT protein autonomously catalyzes transport of its own passenger across the OM (Loveless and Saier, 1997; Henderson et al., 1998), other studies have cast doubt on this model (Bernstein, 2007). Moreover, in the absence of a significant quantity of ATP or a proton gradient across the OM, the molecular driving force for efficient OM secretion remains unclear (Thanassi et al., 2005).

Molecular driving forces are integral components of diverse cellular processes, including transport of cargo along microtubules by kinesin, the separation of double-stranded nucleic acid structures, and the unfolding of substrate proteins prior to their degradation (Zolkiewski, 2006; Enemark and Joshua-Tor, 2008; Zhang et al., 2009; Martin et al., 2010; Myong and Ha, 2010). In each of these examples, molecular motors use the chemical energy of ATP hydrolysis to produce an asymmetrical conformational change, which is used to produce a mechanical force. Similarly, ions and small molecules can be concentrated inside cells by symporters, which use the release of an electrochemical potential as the energy source to drive gated conformational changes (Abramson and Wright, 2009; Krishnamurthy et al., 2009). But given that there is essentially no ATP nor a proton gradient available to drive secretion across the OM, it is currently unclear how directed motion of AT passengers across the OM is achieved.

It is now clear that AT secretion is facilitated by the highly conserved and essential outer membrane protein BamA (Voulhoux et al., 2003; Jain and Goldberg, 2007; Ieva and Bernstein, 2009; Sauri et al., 2009), which is known to facilitate insertion of many integral outer membrane protein (OMP) domains into the OM. It is still unclear, however, whether AT proteins rely on BamA and/or other host proteins for porin domain insertion only, or whether these host proteins also play direct roles in the transport of the AT passenger across the OM. Defining the contributions of these proteins to passenger transport across the OM *in vivo* is challenging, in part due to their broad substrate specificities and overlapping functional roles (Sklar et al., 2007). As an alternative approach, here we directly test the role of the AT passenger itself in OM secretion by investigating the contributions of passenger stability and folding properties to OM secretion.

For this analysis, we used two well-studied ATs: pertactin (from *Bordetella pertussis*) (Leininger et al., 1991) and plasmid-encoded toxin (Pet, from a pathogenic strain of *E. coli*) (Navarro-Garcia et al., 2001) (Figure 1A&C). The 60 kDa pertactin passenger is composed entirely of β-helical structure (Emsley et al., 1996). In contrast, the larger (100 kDa) Pet passenger also has an N-terminal globular structure, a characteristic feature of the SPATE (serine protease autotransporters of *Enterobacteriaceae*) AT sub-family (Dutta et al., 2002; Otto et al., 2005) and other unrelated AT passengers, including IgA protease (Johnson et al., 2009). Despite low sequence identity, both pertactin and Pet contain a "stable core" of β-helix rungs at the C-terminus of their passengers (Junker et al., 2006; Renn and Clark,

2008). This similar structural organization, coupled with the recent observation that pertactin OM secretion – and extracellular folding – proceeds vectorially from C- to N-terminus (Junker et al., 2009), led us to test how local stability within the AT passenger affects its OM secretion.

Results

OM secretion of an AT passenger is reduced in the presence of a stabilizing, OM-permeable ligand

Despite the widespread appearance of β-helical structure in AT passengers, in all AT crystal structures solved to date the active site or functional region of the mature virulence protein is located in a non-β-helical structure or loop within 300 aa of the passenger N-terminus (Emsley et al., 1996; Otto et al., 2005; Gangwer et al., 2007; Johnson et al., 2009; van den Berg, 2010). We systematically altered the stability of the globular N-terminus of the Pet passenger and determined the corresponding effects on OM secretion efficiency. Initially, we attempted to perform this analysis by mutating the endogenous Pet N-terminal protease structure, but this portion of the passenger alone is highly aggregation-prone, which prohibited calculations of its stability ($\Delta G_{\text{folding}}$).

As an alternative approach, we constructed a chimeric passenger that replaces the N-terminal Pet protease structure with *E. coli* DHFR (Figure 1). At 18 kDa, DHFR is smaller than the endogenous Pet protease structure (30 kDa), but its folding properties are well characterized (Touchette et al., 1986; Jennings et al., 1993). Despite replacement of 25% of the wild type Pet passenger with DHFR, the DHFR-Petβ-helix chimera was secreted into the extracellular milieu (Figure 2A), although accumulation of the passenger+porin precursor in whole cell lysates indicates that its secretion efficiency is somewhat reduced versus wild type Pet. These results are consistent with other reports of the tolerance of the AT secretion mechanism to the transport of heterologous domains (Veiga et al., 2004; Jong et al., 2007; Jose and Meyer, 2007). To test the effects of DHFR folding on OM secretion of this chimera, we first used methotrexate (MTX), an OM-permeable DHFR inhibitor that stabilizes the DHFR native structure and binds only to DHFR native conformations (Touchette et al., 1986). Addition of up to 500 μM MTX to the culture medium had no effect on cell growth or OM secretion of wild type Pet (Figure 2A), but produced a dose-dependent reduction in OM secretion of the chimera, as measured by the reduced extracellular accumulation of the processed passenger in culture media (Figure 2B & S1A). Concomitantly, a band corresponding to a protein the size of the chimera precursor was enhanced by MTX addition (Figure 2A). Because MTX can cross the OM but not IM, and binds selectively to the DHFR native structure (Touchette et al., 1986), these results are consistent with MTX-induced stabilization of the DHFR native structure within the periplasm and a resulting blockade of OM secretion of the DHFR-Petβ-helix chimera. Consistent with this model, a destabilized DHFR mutant (I155A; see Table S1) required higher concentrations of MTX to produce a similar blockade of OM secretion (Figure 2B). These results agree well with studies of other ATs showing that OM secretion can be blocked by ligand binding-induced passenger stabilization (Jong et al., 2007) or the formation of a long disulfide-bonded loop in the periplasm (Junker et al., 2009). Moreover, these results provide clear evidence that DHFR can fold to its native structure in the context of this chimera. Interestingly, however, the reduction of secretion efficiency for the DHFR chimera reached a plateau at 30%, rather than 0%, suggesting that while MTX-induced stabilization of the passenger N-terminus can significantly reduce OM secretion efficiency, a complete blockade could require either additional stability and/or alteration of other factors not related to passenger domain N-terminal stability.

To confirm the location (periplasmic versus extracellular) of DHFR in these secretion stalled chimera constructs, we used fluorescently labeled methotrexate (MTX-FL), which also blocks OM secretion of the chimera (Figure S1B). We incubated *E. coli* with MTX-FL, then expressed a DHFR-Petβ-helix construct mutated to inhibit autocatalytic cleavage of the passenger from its C-terminal porin (Navarro-Garcia et al., 2001); this mutant is transported to the cell surface, but retained there. After expression, we tested the accessibility of DHFR-bound MTX-FL to an anti-flurescein antibody that quenches fluorescein fluorescence and is too bulky (~150 kDa) to diffuse across the OM. We hypothesized that if DHFR is retained within the periplasm, the fluorescence of the bound MTX-FL will be quenched to a lesser extent than for DHFR-MTX-FL exposed on the cell surface. Figure 2C shows that MTX-FL fluorescence in the presence of the uncleavable chimera bearing wild type DHFR is unaffected by the addition of quencher (two-tailed *t*-test; $p = 0.09$; of 80 total cells observed in 10 fields, 68 (85%) were detectably fluorescent in the absence of quencher; of 94 total cells (in four fields) observed in the presence of quencher, 77 (82%) were fluorescent). The inability of the quencher to reduce MTX-FL fluorescence indicates that the majority of the DHFR-MTX-FL is protected within the periplasm. As a control, we also expressed a non-cleavable version of the destabilized DHFR-I155A chimera, which is very efficiently secreted (see below), even in the presence of low concentrations of MTX (Figure 2B). MTX-FL fluorescence is efficiently quenched in the presence of this destabilized, efficiently secreted chimera (Figure 2C; of 85 total unquenched cells in six fields, 75 (88%) were detectably fluorescent, but in the presence of quencher only one of 58 (2%) total cells in five fields was fluorescent; $p < 0.0001$). These results confirm that folded DHFR, stabilized by binding to MTX, is retained within the periplasm.

OM secretion of DHFR-Petβ-helix is linearly correlated with DHFR stability

If stabilization of the N-terminal DHFR can block OM secretion of the chimera, we wondered whether reducing DHFR stability would enhance OM secretion. A number of point mutants with a wide range of effects on DHFR stability and folding properties have been characterized (Table S1) (Perry et al., 1987; Garvey and Matthews, 1989; Arai et al., 2003). When introduced into the DHFR-Petβ-helix chimera, mutations that destabilize DHFR led to increased OM secretion and processing of the chimera (Figure 3). Conversely, point mutations that stabilize DHFR led to reduced OM secretion and processing (Figure 3), analogous to the effect observed upon addition of MTX. Overall, altering passenger domain N-terminal stability produced a linearly correlated ($R = 0.83$) change in OM secretion efficiency. To further test the idea that OM secretion efficiency can be controlled by the stability of the AT passenger domain N-terminus, we also designed a highly destabilized F31D/I155A double mutant that does not form stable structure even at 0 M urea ($\Delta G_{folding} > 0$ kJ/mol; see Figure S2A), as measured by pulse proteolysis (Park and Marqusee, 2005). As expected, this highly destabilized mutant is secreted to even higher levels (Figure 3), similar to a Pet passenger variant with the N-terminal protease structure deleted (PetΔprotease; Renn & Clark, 2008). Moreover, even if the chimera chimera context alters the absolute stability of DHFR, since we are comparing point mutants within the chimera context it is unlikely that this would affect the general trend observed here.

DHFR folding kinetics are complex, but we observed a closer correlation between OM secretion efficiency and DHFR stability than with the rate-limiting DHFR folding or unfolding rates, or the position of the mutation in the DHFR sequence (Figure S2B–D). For some DHFR mutations, we also detected smaller Pet chimera fragments (not shown); however, the correlation between DHFR stability and OM secretion efficiency persisted regardless of whether these fragments were included in the analysis ($R = 0.77$), or not ($R = 0.83$; above). Moreover, immunofluorescence microscopy revealed that the more stable chimeras are detected as punctate foci at the bacterial cell surface (Figure 4D). Analogous to

the MTX-FL results above (Figure 2C), these foci presumably represent stalled OM secretion intermediates where the C-terminal Pet β-helix portion of the passenger has been secreted (and is accessible to the anti-Pet antibody), but the construct is retained at the surface due to the inability to secrete the bulky, stably folded N-terminal DHFR portion of the passenger. In contrast, chimeras bearing less stable DHFR variants (including wild type DHFR) are not detectable at the cell surface (Figure 4C&E), presumably due to their release into culture media at the successful conclusion of OM secretion.

The stabilizing DHFR mutations also result in increased accumulation of a band corresponding to the size of the unprocessed chimera precursor (passenger+porin) in whole cell lysates (Figure S2E), whereas less stable DHFR variants do not produce a detectable unprocessed band (Figure S2E). These results are consistent with the interpretation that increased passenger domain N-terminal stability impedes transport across the OM, rather than an earlier step in autotransporter biogenesis. Indeed, an identical correlation ($R = 0.83$) was found between $\Delta G_{folding}$ and the fraction of protein secreted (i.e., (amount secreted)/(total protein detected in media plus cells); Figure S2F). In other words, DHFR stabilization led to increased intracellular accumulation of unprocessed pre-protein and decreased extracellular accumulation of the chimera, while DHFR destabilization produced the opposite result.

Destabilization of the pertactin C-terminal stable core dramatically lowers OM secretion efficiency

To test the contributions of the folding properties of β-helical portions of the AT passenger to OM secretion, we turned to pertactin, the only naturally occurring AT passenger domain known to unfold and refold reversibly at equilibrium (Junker et al., 2006). Similar to Pet, the pertactin passenger domain is also cleaved from its C-terminal porin via an intramolecular cleavage reaction within its C-terminal porin (Dautin et al., 2007), but unlike Pet, the processed pertactin passenger domain remains tightly associated with the outer surface of the bacterial cell (Junker et al., 2009). *In vitro*, the purified pertactin passenger domain unfolds in two distinct transitions: the N-terminal half of the β-helix unfolds with a melting temperature of 65ºC, while the C-terminal half of the β-helix has a melting temperature of 82ºC (Figure 5A) (Junker et al., 2006). We mutated the pertactin passenger domain to selectively destabilize either the N-terminal half of the β-helix (W295F, destabilizing the first unfolding transition), the C-terminal half (L498K, destabilizing the second unfolding transition) or the entire passenger domain (W423F/W440F, destabilizing both transitions) (Figure 5A).

We introduced the mutations described above into the gene encoding full-length pertactin, and expressed these genes in *E. coli*. This pertactin expression plasmid permits either low-level constitutive expression (via a *tac* promotor) or IPTG-inducible over-expression (Junker et al., 2009). Upon transport across the OM wild type pertactin is auto-catalytically cleaved from the C-terminal porin to produce the mature, extracellular passenger domain from the larger pertactin precursor (Figure 5B) (Junker et al., 2009). Similarly, the W295F mutation that destabilizes only the N-terminus of the passenger domain β-helix resulted in significant extracellular accumulation of the processed pertactin passenger domain, at levels comparable to wild type pertactin, regardless of growth conditions (Figure 5B). In contrast, mutations that destabilize either the C-terminal “stable core” portion of the passenger domain or globally destabilized the entire passenger domain greatly reduced OM secretion under all growth conditions (Figure 5B), while having no effect on IPTG-induced production of the unprocessed pertactin precursor (Figure 5B, white arrowhead). It is important to note that in contrast to the Pet chimera constructs characterized above, blocking pertactin OM secretion under low expression conditions does not lead to increased precursor accumulation, presumably because the rate of degradation of these precursors is similar to

the rate of OM secretion. Crucially, examining pertactin secretion under different growth conditions demonstrates that the different levels of processed pertactin detected here are not due to differences in protein production. This is most noticeable upon the over-expression in the presence of IPTG, where the pertactin precursor accumulates to the same level regardless of mutation, suggesting that there are no significant differences in expression of these constructs. These results indicate that, in striking contrast to the globular N-terminal domain, AT passenger β-helix stability positively contributes to OM secretion efficiency, with the stability of the C-terminal stable core making the most dramatic contributions to secretion efficiency.

The pertactin passenger N-terminus is incapable of folding *in vitro*

Although the pertactin passenger enters the periplasm from N- to C-terminus, we have previously shown that the passenger exits the periplasm by crossing the OM from C- to N-terminus (Junker et al., 2009). This raises the question of what prevents the premature folding of the pertactin passenger N-terminus upon entry into the periplasm. We have shown that complete, native-like folding the entire pertactin passenger domain is an extremely slow process *in vitro* ($t_{1/2}$ ~ hours), but is preceded by the formation of intermediates with significant β-sheet structure throughout the passenger domain (Junker and Clark, 2010). To study the intrinsic folding capacity of the pertactin N-terminus, we designed a construct corresponding to the less-stable N-terminus of the passenger domain (residues 1–334) (Junker et al., 2006). *In vitro*, the pertactin passenger domain N-terminus has “random coil” spectral signatures, as measured by far-UV circular dichroism (no characteristic β-sheet minimum at 218 nm) and fluorescence emission spectroscopy (no denaturant-dependant changes to the fluorescence spectrum) (Figure 6). These results suggest that folding of the pertactin passenger domain is unlikely to be initiated at the N-terminus upon entry into the periplasm.

Discussion

Transport of AT virulence proteins across the OM is one example of a molecular machine that produces a driving force, or directed motion. In comparison to undirected motion (such as Brownian motion, arising from the thermal fluctuations that affect all biomolecules), directed motion requires an anisotropic potential (Astumian, 1997). The results reported here demonstrate that AT passenger secretion across the OM is dependent on an anisotropic distribution of stability within the passenger domain: high stability at the passenger C-terminal βhelix facilitates OM secretion, as does low stability at the globular N-terminus. Interestingly, selectively altering the stability of the N-terminal half of the passenger β-helix, as we were able to do for pertactin, had no significant effect on OM secretion, suggesting this region might represent a neutral “fulcrum” in the anisotropic distribution of passenger domain stability and therefore play a different role in autotransporter function (note that for both pertactin and Pet, sequences within the N-terminus of the β-helix are known to make functional contributions to virulence (Leininger et al., 1991; Dutta et al., 2003)). For both pertactin and Pet, the C-terminus of the wild type passenger domain is more stable than the N-terminus (Junker et al., 2006; Renn and Clark, 2008), and we show here that selectively destabilizing this “stable core” drastically impedes OM secretion. The correlations between the anisotropic distribution of AT passenger stability and its effects on OM secretion efficiency demonstrate that passenger domain folding properties are directly connected to the mechanism of OM secretion, and that AT passenger domains contain specific folding properties that facilitate their secretion across the OM.

What is the mechanistic role for these regionalized differences of passenger domain stability, and their effects on OM secretion? We hypothesize that AT passenger domains cross the OM by exploiting the internal anisotropy of passenger domain stability, which

enforces a direction over an otherwise directionless Brownian motion. In other words, placement of a folding-competent portion of the passenger β-helical C-terminus in the extracellular milieu as part of β-domain porin insertion (Figure 7, facilitated by BamA) could drive secretion of the passenger domain across the OM, via a unique, ATP-independent Brownian ratchet mechanism driven by the folding of the passenger domain C-terminus. In contrast to well-studied catalytic motors driven by ATP hydrolysis (such as the mechanism by which myosin "walks" along actin), each AT folding transporter is used only once, to transport a single passenger domain. Moreover, after the passenger domain is transported across the OM, it is typically cleaved from its C-terminal porin (often via an intramolecular reaction within the porin), rendering this motion irreversible. Essentially, the free energy of folding provides a "pawl" (latch) for a Brownian ratchet, creating a folding-driven transporter that prevents backsliding of the passenger into the periplasm. It is also important to note that these results establish a surprising correlation between an equilibrium state function ($\Delta G_{folding}$) and a non-equilibrium process (dynamic transport through the periplasm and across the OM).

While a few studies have reported successful OM secretion of folded heterologous passenger domain structures (Veiga et al., 2004; Skillman et al., 2005) and small disulfide-bonded loops (Jong et al., 2007), there appears to be a growing consensus that formation of larger, stably folded structure within the periplasm is incompatible with AT OM secretion (Klauser et al., 1990; Jose et al., 1996; Jong et al., 2007; Junker et al., 2009; Leyton et al., 2011). Results presented here demonstrate that periplasmic folding of a globular domain at the AT passenger N-terminus reduces OM secretion efficiency. But what prevents a wild type AT passenger from adopting a stable structure prematurely in the periplasm? *In vivo*, the passenger enters the periplasm from N- to C-terminus, in contrast to OM secretion, which proceeds from C- to N-terminus (Junker et al., 2009). Our results suggest that the pertactin N-terminus is incapable of initiating folding (Figure 6), which might retard the folding rate in the periplasm. These results might explain why a recent study of OM secretion of EspP (a homolog of Pet) reported that EspP passenger domain constructs with faster *in vitro* refolding kinetics were secreted *more* efficiently across the OM, rather than less (Peterson et al., 2010). Regardless of the precise mechanism, the environment for initiating AT passenger folding in the periplasm (or the test tube) appears fundamentally different from the extracellular environment and incompatible with the rapid formation of stable structure within the AT passenger N-terminus before OM secretion.

Given that OM secretion appears to require the passenger N-terminus to maintain or adopt an destabilized conformation in the periplasm, the crucial variables for the N-terminal domain will be the relative stabilities of the folded and unfolded states ($\Delta G_{folding}$) and – remembering that the periplasm is a non-equilibrium system (Clark, 2004) – the rate at which the unfolded state can be accessed from the folded state (k_{unf}; see Figure S1C). Of course, these variables must remain compatible with the native state stability required for activity of the mature passenger domain (Bloom et al., 2006). Finally, while the correlation reported here between regionalized AT passenger stability and OM secretion efficiency highlights one aspect of the AT OM secretion mechanism, it is important to note that many other factors surrounding this mechanism remain unclear. For example, it has been shown that small (but not large) disulfide-bonded loops within the AT passenger can be efficiently secreted across the OM, suggesting a limited tolerance to periplasmic folding within the passenger (Jong et al., 2007; Leyton et al., 2011). Moreover, interactions between AT OM secretion precursors and periplasmic chaperones could further modulate the effects observed here, for example by stabilizing unfolded conformations of AT precursors while they transit the periplasm.

Significance

Here, we modulated OM secretion efficiency by manipulating the biophysical properties of the transported AT passenger. These results indicate that the folding properties of distinct regions of the AT passenger provide a directed molecular driving force, for use as a generalized transporter device. Strategies that alter AT passenger folding properties might therefore be effective for combating Gram-negative bacterial pathogenesis. In addition, the contributions of the passenger folding properties to secretion efficiency have significant implications for the re-engineering of the AT secretion mechanism for transport of heterologous protein "cargo", such as for *in vitro* protein evolution ("auto-display") (Jose and Meyer, 2007). In conclusion, the regionalized distribution of AT passenger domain stability provides a unique solution for the directed transport of macromolecules across biological membranes, suggesting a new, ATP-independent category of folding-driven transporter.

Materials and Methods

Molecular biology

pET21b-PetΔprotease was constructed using an approach analogous to the one used to construct pCEFN1Δprotease (Renn and Clark, 2008). *E. coli* DHFR C85A/C152S was amplified from plasmid pTZ-AS-DHFR(Iwakura et al., 1993), using primers that included *Nhe*I overhangs. This PCR product was ligated into the unique *Nhe*I site in pET21-PetΔprotease, located between the sequence encoding the signal sequence and the Pet passenger β-helix. DHFR, Pet, and pertactin point mutants were constructed by site-directed mutagenesis. The sequence of each construct was confirmed by DNA sequencing.

Expression and detection of Pet and Pet chimera constructs

All pET21b-Pet constructs were expressed in *E. coli* strain BL21(DE3)pLysS. Typically, an overnight culture was prepared from a single colony in 25 mL LB plus 100 μg mL^{-1} of ampicillin at 37°C. 250 μL of this overnight culture was diluted into 25 mL LB plus 100 μg mL^{-1} of ampicillin and grown to OD_{600}=0.20–0.25. Expression was initiated by addition of 0.5 mM IPTG. After 50 min, the cell culture was centrifuged at 5000×*g* for 5 min to separate the cells from the spent media. The spent media was filtered through a 0.22 μm filter and 1.5 mL was precipitated with 20% trichloroacetic acid. The cell pellet was resuspended in SDS gel loading buffer, and lysed by a single freeze/thaw step. Proteins present in the media and cell fractions were analyzed by SDS-PAGE and western blotting using an anti-Pet polyclonal antibody as follows. Proteins were transferred to a PVDF membrane, typically for 1 hr at 75 V in buffer containing 25 mM Tris, 192 mM glycine and 20% methanol. Non-specific antibody binding was reduced by incubating for 10 min with 5% powdered dry milk (PDM) in Tris-buffered saline plus Tween-20 (TBST; 20 mM Tris pH 7.5, 150 mM NaCl and 0.5% Tween-20). The membrane was incubated for 45 min in a solution containing an anti-Pet passenger polyclonal antibody in 5% PDM in TBST, followed by a 30 min incubation with a solution containing an alkaline phosphatase-conjugated anti-rabbit secondary antibody (Novus Biologicals) in TBST containing 5% PDM. For both the primary and secondary antibody, excess unbound antibody was removed by three washes with TBST for 90 sec each. The membrane was washed five times with double deionized water, and bands were visualized by incubating the membrane in nitro-blue tetrazolium chloride (NBT) and bromo-chloro-indolyl-phosphate (BCIP) substrates (Promega) in alkaline phosphotase (AP) buffer, typically for 5 to 10 min. The AP buffer contained 100 mM Tris pH 9.0, 100 mM NaCl, and 5 mM $MgCl_2$. Blots were quantified as described below.

Methotrexate titration of DHFR-Petβ-helix secretion

Methotrexate (MTX; Sigma) and fluorescein-conjugated methotrexate (MTX-FL; Invitrogen) were prepared as 10 mg/mL and 2 mg/mL stock solutions, respectively, in 0.1 M NaOH. Three milliliters of a log phase culture of *E. coli* (OD_{600}=0.2–0.25) was prepared as described above and treated with MTX or MTX-FL to achieve the indicated range of final concentrations. Cultures were incubated with MTX (or FL-MTX) for 10 min at 37°C while shaking, followed by IPTG-induced induction of expression of DHFR-Petβ-helix (bearing either wild type DHFR, or the destabilizing I155A mutation). Accumulation of DHFR-Petβ-helix in the spent media and whole cells was analyzed as described above.

Quantification of autotransporter secretion efficiency

Western blot band intensities for Pet passenger domain constructs were measured by densitometry, quantified using NIH ImageJ software, and compared to a standard curve of band intensities of known concentrations of purified PetΔprotease. For all DFHR-Petβ-helix experiments, the ~100 kDa processed passenger band, corresponding to the secreted protein, was quantified from the spent media fraction. For analyzing the effect of MTX on DHFR-Petβ-helix secretion, results were normalized to 0 nM MTX (100% secretion). For DHFR chimera mutants, the band corresponding to the DHFR-Petβ-helix passenger domain was quantified for at least 4 independent experiments each mutant and normalized to the intensity of the band corresponding to the chimera bearing the wild type DHFR sequence; error was calculated as the standard deviation between these measurements. To calculate secretion efficiency as the fraction of the Pet construct that was processed and released from the cell surface relative to all Pet construct detected (released plus cell-associated; Figure S1E&F), we also quantified bands corresponding to the unprocessed pre-protein in the whole cell lysate fraction for three independent experiments. For these experiments, secretion efficiency was calculated as follows:

$$\text{secretion efficiency} = \frac{\text{passenger band intensity}}{\text{passenger band intensity} + \text{precursor band intensity}}$$

Fluorescence microscopy

For detection of MTX-FL fluorescence, 500 μL of a log-phase culture of *E. coli* BL21 transformed with empty vector or a plasmid encoding a DHFR-Petβ-helix construct was incubated with FL-MTX (1 nM final concentration) for 10 min. Protein expression was induced by addition of IPTG to a final concentration of 0.5 mM, followed by 30 min incubation at 37°C. Cells were harvested by centrifugation at 1000×*g* for 5 min, washed twice with phosphate buffered saline (PBS) to remove excess, unbound FL-MTX. Resuspended cells were diluted five-fold, and divided into two groups of 500 μL aliquots. To one group, 5 μL of the anti-fluorescein quencher (anti-fluorescein/Oregon Green rabbit IgG; Invitrogen) was added. To the other group, 5 μL of PBS was added. Aliquots were incubated for 20 min in the dark, after which cells were immobilized on poly-L-lysine-coated cover slips for 20 min. Cover slips were washed twice with PBS to remove unbound quencher. Microscopy images were collected using an Applied Precision DeltaVision Core fluorescence microscope, using identical conditions for each construct (1.42 numerical aperture, 100X objective, and 40 ms exposure time). The fluorescence images were deconvolved using constrained iterative deconvolution. For the quantification, the total number of cells visible in the bright field image was counted for each field, and the number of detectably fluorescent cells was expressed as a percentage of this total. There was no significant difference in fluorescence of unquenched cells expressing either the wild type DHFR or DHFR-I155A chimera (p = 0.158).

For immunofluorescence detection of DHFR-Petβ-helix localization, log-phase cell cultures of *E. coli* BL21 expressing different DHFR-Petβ-helix constructs, a non-cleavable PetΔprotease mutant (N1018G/N1019I), or the empty vector were induced for 30 min, harvested by centrifugation at 1000×*g* for 5 min, resuspended in PBS, and washed twice with PBS to remove secreted, cleaved Pet passenger constructs. Resuspended cells were placed on poly-L-lysine coated cover slips, followed by a 10 min incubation with the anti-Pet polyclonal antibody and a 10 min incubation with a Cy3 conjugated anti-rabbit secondary antibody (Jackson ImmunoResearch Labs, West Grove, PA). Each antibody incubation was preceded by three washes with PBS; prior to imaging, three final washes were performed. Images were collected as described above.

Pertactin expression and quantification

Pertactin passenger domain expression, purification, and optical spectra (far-UV circular dichroism and tryptophan fluorescence) were performed and collected as previously described (Junker et al., 2006; Junker and Clark, 2010). Expression and extracellular secretion of full-length pertactin and its mutants was performed as previously described (Junker et al., 2009). Briefly, for wild type pertactin and each mutant, anti-pertactin western blot bands corresponding to the 60 kDa extracellular processed passenger domain (closed arrowhead in Figure 5B) and the 93 kDa unprocessed precursor (passenger+porin; open arrowhead in Figure 5B) were quantified using the public domain NIH ImageJ program. Secretion of wild type pertactin, as measured by the intensity of the processed passenger, was set at 100%. Secretion of the mutant pertactin constructs is expressed as a percentage of wild type pertactin secretion.

Supplementary Material

Refer to Web version on PubMed Central for supplementary material.

Acknowledgments

We thank M. Finn and Tatiana Quiñones Ruiz for technical assistance, J. Peng for helpful discussions, and C.R. Matthews and A. Matouschek for helpful discussions of DHFR mutants and folding properties. The *E. coli* DHFR expression plasmid was a kind gift from C.R. Matthews. This work was supported by an NSF CAREER grant (MCB 0237945). J.P.R. and E.B. were supported by an NIH training fellowship (T32 GM075762).

References

Abramson J, Wright EM. Structure and function of Na(+)-symporters with inverted repeats. Curr Opin Struct Biol. 2009; 19:425–432. [PubMed: 19631523]

Arai M, Maki K, Takahashi H, Iwakura M. Testing the relationship between foldability and the early folding events of dihydrofolate reductase from Escherichia coli. J Mol Biol. 2003; 328:273–288. [PubMed: 12684013]

Astumian RD. Thermodynamics and kinetics of a Brownian motor. Science. 1997; 276:917–22. [PubMed: 9139648]

Bernstein HD. Are bacterial 'autotransporters' really transporters? Trends Microbiol. 2007; 15:441–447. [PubMed: 17935998]

Bloom JD, Labthavikul ST, Otey CR, Arnold FH. Protein stability promotes evolvability. Proc Natl Acad Sci USA. 2006; 103:5869–5874. [PubMed: 16581913]

Clark PL. Protein folding in the cell: Reshaping the folding funnel. Trends Biochem Sci. 2004; 29:527–534. [PubMed: 15450607]

Dutta PR, Cappello R, Navarro-Garcia F, Nataro JP. Functional comparison of serine protease autotransporters of enterobacteriaceae. Infect Immun. 2002; 70:7105–7113. [PubMed: 12438392]

Dutta PR, Sui BQ, Nataro JP. Structure-function analysis of the enteroaggregative *Escherichia coli* plasmid-encoded toxin autotransporter using scanning linker mutagenesis. J Biol Chem. 2003; 278:39912–39920. [PubMed: 12878602]

Emsley P, Charles IG, Fairweather NF, Isaacs NW. Structure of *Bordetella pertussis* virulence factor P.69 pertactin. Nature. 1996; 381:90–92. [PubMed: 8609998]

Enemark EJ, Joshua-Tor L. On helicases and other motor proteins. Curr Opin Struct Biol. 2008; 18:243–257. [PubMed: 18329872]

Gangwer KA, Mushrush DJ, Stauff DL, Spiller B, McClain MS, Cover TL, Lacy DB. Crystal structure of the Helicobacter pylori vacuolating toxin p55 domain. Proc Natl Acad Sci USA. 2007; 104:16293–16298. [PubMed: 17911250]

Garvey EP, Matthews CR. Effects of multiple replacements at a single position on the folding and stability of dihydrofolate reductase from Escherichia coli. Biochemistry. 1989; 28:2083–2093. [PubMed: 2655702]

Henderson IR, Navarro-Garcia F, Nataro JP. The great escape: Structure and function of the autotransporter proteins. Trends Microbiol. 1998; 6:370–378. [PubMed: 9778731]

Ieva R, Bernstein HD. Interaction of an autotransporter passenger domain with BamA during its translocation across the bacterial outer membrane. Proc Natl Acad Sci USA. 2009; 106:19120–19125. [PubMed: 19850876]

Iwakura M, Jones BE, Falzone CJ, Matthews CR. Collapse of parallel folding channels in dihydrofolate reductase from *Escherichia coli* by site-directed mutagenesis. Biochemistry. 1993; 32:13566–13574. [PubMed: 8257692]

Jain S, Goldberg MB. Requirement for YaeT in the outer membrane assembly of autotransporter proteins. J Bacteriol. 2007; 189:5393–5398. [PubMed: 17513479]

Jennings PA, Finn BE, Jones BE, Matthews CR. A reexamination of the folding mchanism of dihydrofolate reductase from *Escherichia coli*: Verification and refinement of a 4-channel model. Biochemistry. 1993; 32:3783–3789. [PubMed: 8466916]

Johnson TA, Qiu J, Plaut AG, Holyoak T. Active-site gating regulates substrate selectivity in a chymotrypsin-like serine protease the structure of Haemophilus influenzae immunoglobulin A1 protease. J Mol Biol. 2009; 389:559–574. [PubMed: 19393662]

Jong WS, ten Hagen-Jongman CM, den Blaauwen T, Jan Slotboom D, Tame JR, Wickstrom D, de Gier JW, Otto BR, Luirink J. Limited tolerance towards folded elements during secretion of the autotransporter Hbp. Mol Microbiol. 2007; 63:1524–1536. [PubMed: 17302825]

Jose J. Autodisplay: efficient bacterial surface display of recombinant proteins. Appl Microbiol Biotechnol. 2006; 69:607–614. [PubMed: 16369779]

Jose J, Kramer J, Klauser T, Pohlner J, Meyer TF. Absence of periplasmic DsbA oxidoreductase facilitates export of cysteine-containing passenger proteins to the Escherichia coli cell surface via the Iga beta autotransporter pathway. Gene. 1996; 178:107–110. [PubMed: 8921899]

Jose J, Meyer TF. The autodisplay story, from discovery to biotechnical and biomedical applications. Microbiol Mol Biol Rev. 2007; 71:600–619. [PubMed: 18063719]

Junker M, Besingi RN, Clark PL. Vectorial transport and folding of an autotransporter virulence protein during outer membrane secretion. Mol Microbiol. 2009; 71:1323–1332. [PubMed: 19170888]

Junker M, Clark PL. Slow formation of aggregation-resistant β-sheet folding intermediates. Proteins: Struct Funct Bioinf. 2010; 78:812–824.

Junker M, Schuster CC, McDonnell AV, Sorg KA, Finn MC, Berger B, Clark PL. Pertactin β-helix folding mechanism suggests common themes for the secretion and folding of autotransporter proteins. Proc Natl Acad Sci USA. 2006; 103:4918–4923. [PubMed: 16549796]

Kajava AV, Cheng N, Cleaver R, Kessel M, Simon MN, Willery E, Jacob-Dubuisson F, Locht C, Steven AC. β-helix model for the filamentous haemagglutinin adhesin of *Bordetella pertussis* and related bacterial secretory proteins. Mol Microbiol. 2001; 42:279–292. [PubMed: 11703654]

Klauser T, Pohlner J, Meyer TF. Extracellular transport of cholera toxin B subunit using *Neisseria* IgA protease β-domain: Conformation-dependent outer membrane translocation. EMBO J. 1990; 9:1991–1999. [PubMed: 2189728]

Krishnamurthy H, Piscitelli CL, Gouaux E. Unlocking the molecular secrets of sodium-coupled transporters. Nature. 2009; 459:347–355. [PubMed: 19458710]

Leininger E, Roberts M, Kenimer JG, Charles IG, Fairweather N, Novotny P, Brennan MJ. Pertactin, an Arg-Gly-Asp-containing *Bordetella pertussis* surface protein that promotes adherence of mammalian cells. Proc Natl Acad Sci USA. 1991; 88:345–349. [PubMed: 1988935]

Leyton DL, Sevastsyanovich YR, Browning DF, Rossiter AE, Wells TJ, Fitzpatrick RE, Overduin M, Cunningham AF, Henderson IR. Size and conformation limits to secretion of disulfide-bonded loops in autotransporter proteins. J Biol Chem. 2011 in press.

Loveless BJ, Saier MH Jr. A novel family of channel-forming, autotransporting, bacterial virulence factors. Mol Membr Biol. 1997; 14:113–123. [PubMed: 9394291]

Martin DS, Fathi R, Mitchison TJ, Gelles J. FRET measurements of kinesin neck orientation reveal a structural basis for processivity and asymmetry. Proc Natl Acad Sci USA. 2010; 107:5453–5458. [PubMed: 20212149]

Myong S, Ha T. Stepwise translocation of nucleic acid motors. Curr Opin Struct Biol. 2010; 20:121–127. [PubMed: 20061135]

Navarro-Garcia F, Canizalez-Roman A, Luna J, Sears C, Nataro JP. Plasmid-encoded toxin of enteroaggregative Escherichia coli is internalized by epithelial cells. Infect Immun. 2001; 69:1053–1060. [PubMed: 11160002]

Otto BR, Sijbrandi R, Luirink J, Oudega B, Heddle JG, Mizutani K, Park SY, Tame JR. Crystal structure of hemoglobin protease, a heme binding autotransporter protein from pathogenic Escherichia coli. J Biol Chem. 2005; 280:17339–17345. [PubMed: 15728184]

Park C, Marqusee S. Pulse proteolysis: a simple method for quantitative determination of protein stability and ligand binding. Nat Methods. 2005; 2:207–212. [PubMed: 15782190]

Perry KM, Onuffer JJ, Touchette NA, Herndon CS, Gittelman MS, Matthews CR, Chen JT, Mayer RJ, Taira K, Benkovic SJ. Effect of single amino acid replacements on the folding and stability of dihydrofolate reductase from Escherichia coli. Biochemistry. 1987; 26:2674–2682. [PubMed: 3300767]

Peterson JH, Tian P, Ieva R, Dautin N, Bernstein HD. Secretion of a bacterial virulence factor is driven by the folding of a C-terminal segment. Proc Natl Acad Sci USA. 2010; 107:17739–17744. [PubMed: 20876094]

Renn JP, Clark PL. A conserved stable core structure in the passenger domain β-helix of autotransporter virulence proteins. Biopolymers. 2008; 89:420–427. [PubMed: 18189304]

Sauri A, Soprova Z, Wickstrom D, de Gier JW, Van der Schors RC, Smit AB, Jong WS, Luirink J. The Bam (Omp85) complex is involved in secretion of the autotransporter haemoglobin protease. Microbiology. 2009; 155:3982–3991. [PubMed: 19815580]

Skillman KM, Barnard TJ, Peterson JH, Ghirlando R, Bernstein HD. Efficient secretion of a folded protein domain by a monomeric bacterial autotransporter. Mol Microbiol. 2005; 58:945–958. [PubMed: 16262782]

Sklar JG, Wu T, Kahne D, Silhavy TJ. Defining the roles of the periplasmic chaperones SurA, Skp, and DegP in Escherichia coli. Genes Dev. 2007; 21:2473–2484. [PubMed: 17908933]

Thanassi DG, Stathopoulos C, Karkal A, Li H. Protein secretion in the absence of ATP: The autotransporter, two-partner secretion and chaperone/usher pathways of gram-negative bacteria. Mol Membr Biol. 2005; 22:63–72. [PubMed: 16092525]

Touchette NA, Perry KM, Matthews CR. Folding of dihydrofolate reductase from Escherichia coli. Biochemistry. 1986; 25:5445–5452. [PubMed: 3535877]

van den Berg B. Crystal structure of a full-length autotransporter. J Mol Biol. 2010; 396:627–633. [PubMed: 20060837]

Veiga E, de Lorenzo V, Fernandez LA. Structural tolerance of bacterial autotransporters for folded passenger protein domains. Mol Microbiol. 2004; 52:1069–1080. [PubMed: 15130125]

Voulhoux R, Bos MP, Geurtsen J, Mols M, Tommassen J. Role of a highly conserved bacterial protein in outer membrane protein assembly. Science. 2003; 299:262–265. [PubMed: 12522254]

Zhang F, Hu M, Tian G, Zhang P, Finley D, Jeffrey PD, Shi Y. Structural insights into the regulatory particle of the proteasome from Methanocaldococcus jannaschii. Mol Cell. 2009; 34:473–484. [PubMed: 19481527]

Zolkiewski M. A camel passes through the eye of a needle: protein unfolding activity of Clp ATPases. Mol Microbiol. 2006; 61:1094–1100. [PubMed: 16879409]

Highlights

- Protein stability at N- and C-termini have opposing effects on autotransporter secretion
- Highly secreted proteins are less stable at N-terminus, more stable at C-terminus
- Unexpected correlation between equilibrium state function and biological mechanism
- Suggests novel folding-driven mechanism for ATP-independent protein secretion

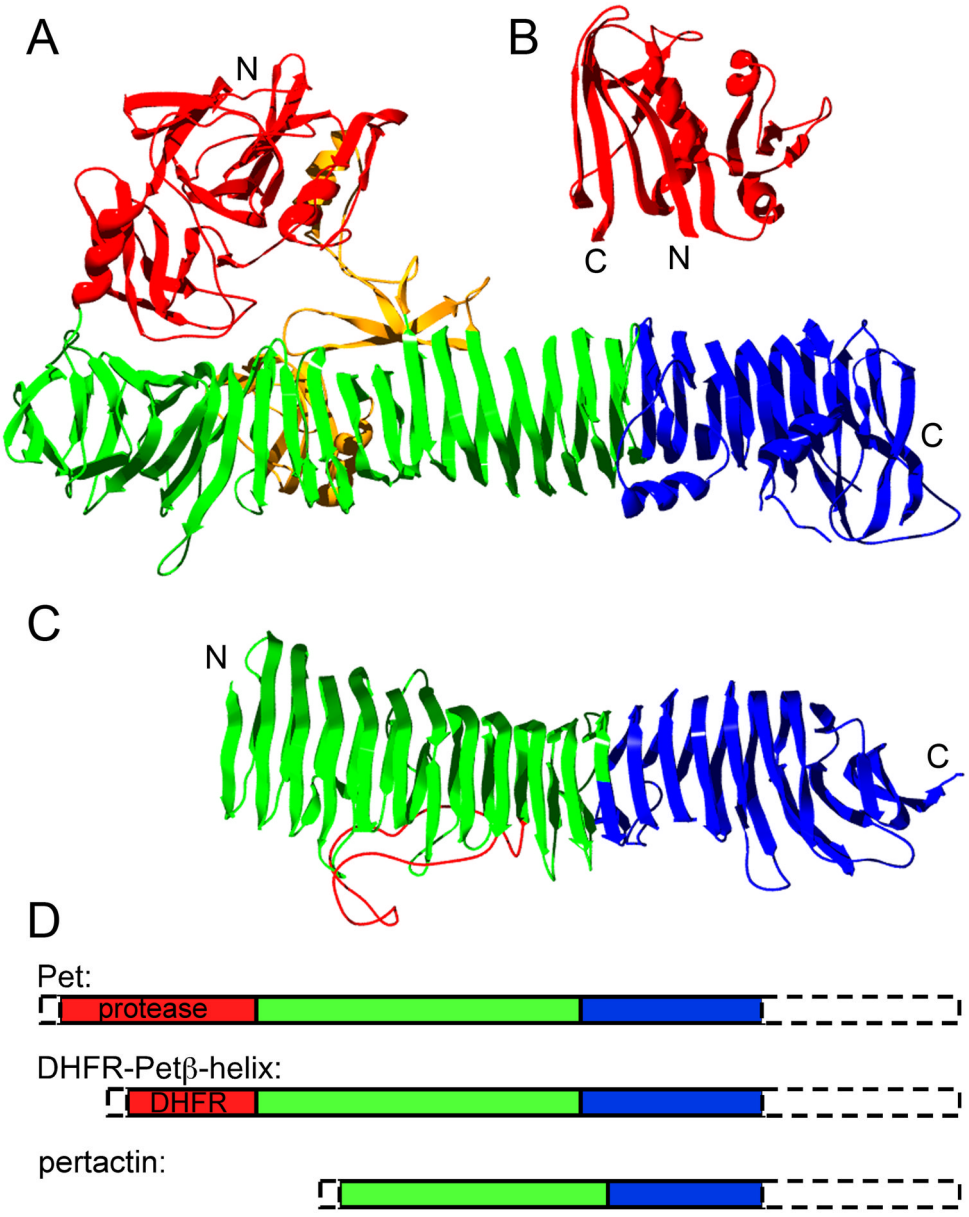

Figure 1.

Structural organization of AT passenger domains, and DHFR. (**A**) Crystal structure of hemoglobin protease passenger (PDB ID: 1WXR), a homolog of Pet (26% identical, 43% similar), (**B**) *E. coli* dihydrofolate reductase (PDB ID: 7DFR), and (**C**) pertactin passenger (PDB ID: 1DAB). The stable core structures of Pet and pertactin are shown in blue, with other βhelical structure in green. Regions associated with function (Pet protease domain and proposed pertactin integrin binding loop) are shown in red, and other, non-β-helical structure is in yellow. (**D**) Schematic representation of the sizes of passenger domain structures and C-terminal stable cores for constructs expressed in this study. The N-terminal signal sequence and C-terminal 30 kDa β-domain porin of each preprotein construct are indicated by dashed lines. See also Supplementary Table 1.

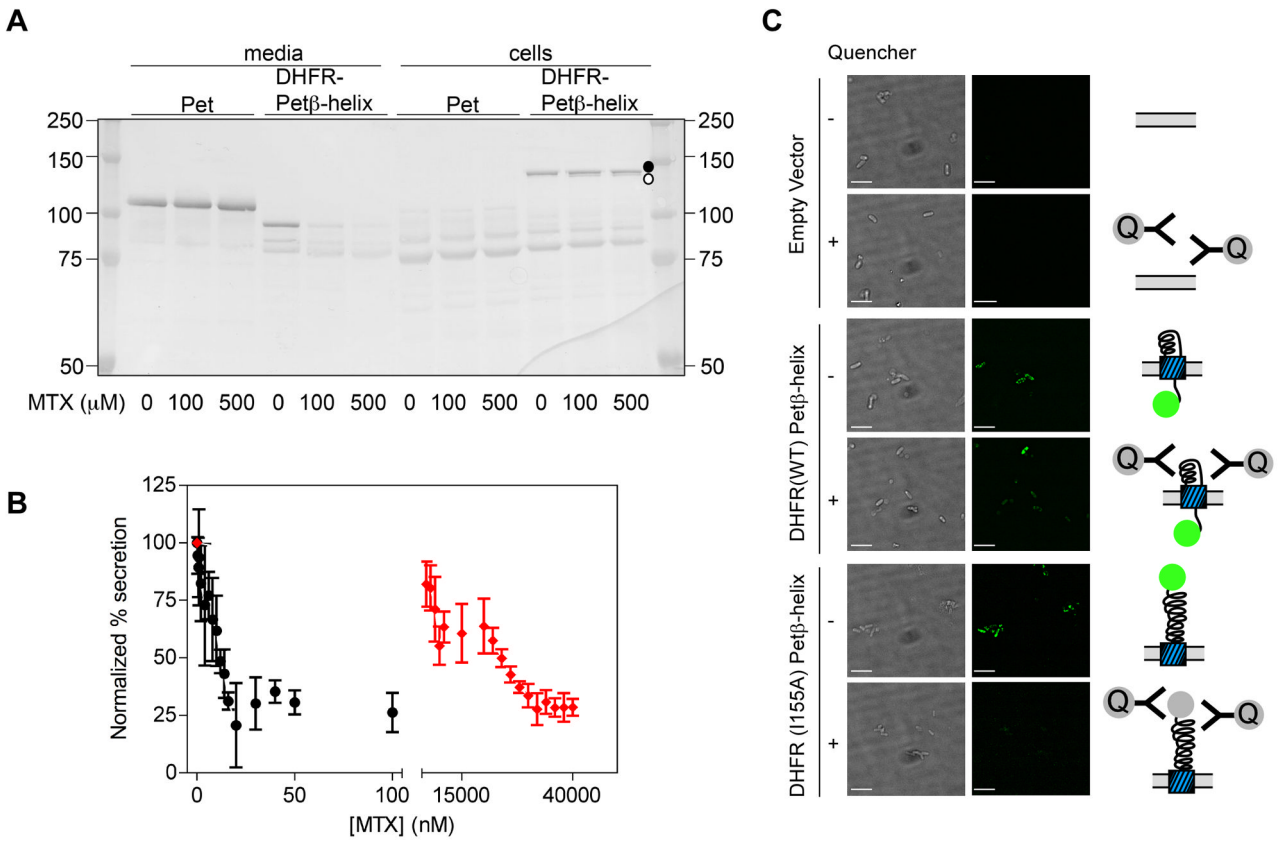

Figure 2.

DHFR stabilization by methotrexate (MTX) blocks OM secretion of DHFR-Petβ-helix. (**A**) MTX does not inhibit secretion of wild type Pet into the spent media (>100 kDa band, left), but does reduce secretion of DHFR-Petβ-helix chimera (<100 kDa band, middle). A band corresponding to the unprocessed DHFR-Petβ-helix precursor is detectable in whole cell lysates (130 kDa, closed circle, right); moreover, in the presence of MTX, a band corresponding to the size of the DHFR chimera periplasmic precursor was detected in whole cell lysates (slightly smaller, open circle, right). Western blot visualized using an anti-Pet polyclonal antibody; note that removal of the Pet protease domain deletes some pAb binding epitopes in the DHFR-Petβ-helix passenger (Renn & Clark, 2008), which prevents direct comparison of band intensity to that of wild type Pet passenger. (**B**) OM secretion of the DHFR-Petβ-helix chimera is inhibited by MTX in a dose-dependent manner. Black circles: chimera bearing wild type DHFR. Red diamonds: chimera bearing DHFR-I155A, which reduces the stability of DHFR (Table S1), requires higher concentrations of MTX to block secretion. Error bars represent the standard deviation of three independent experiments. (**C**) *E. coli* cultures were pre-incubated with fluorescein-labeled MTX before expression of uncleavable mutants of DHFR-Petβ-helix (N1018G/N1019I; Navarro-Garcia et al., 2001), or the empty vector. MTX-FL stabilizes DHFR in the periplasm, blocking OM secretion of the passenger N-terminus and rendering MTX-FL inaccessible to an OM impermeable quencher. Conversely, DHFR mutant I155A is destabilized, which increases its OM secretion efficiency (Figure 4), and enables quenching of MTX-FL bound to DHFR at the cell surface. Left panel, bright field images of *E. coli* bearing the indicated expression plasmid. Right panel, fluorescein fluorescence images of the same field. Scale bar corresponds to 5 μm. See also Figure S1.

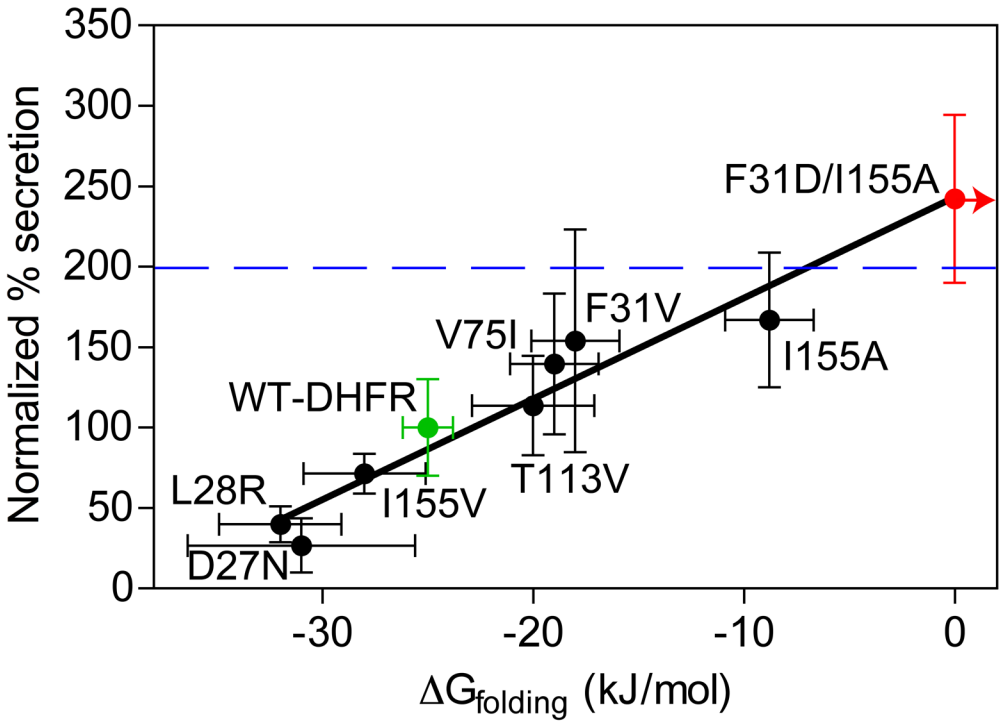

Figure 3.

OM secretion of DHFR-Petβ-helix is dependent on the stability of DFHR. The amount of secreted protein was detected in the spent culture media using an anti-Pet passenger polyclonal antibody, normalized to wild type DHFR (green), and plotted versus the free energy of unfolding of the DHFR domain (measured previously (Perry et al., 1987; Garvey and Matthews, 1989; Arai et al., 2003); see also Table S1). The double mutation with $\Delta G_{folding} > 0$ kJ/mol (see Figure S1A) is shown in blue; the blue arrow indicates $\Delta G_{folding} > 0$ kJ/mol. The linear fit (line) resulted in $R = 0.83$. For comparison, secretion of PetΔprotease, which lacks an N-terminal globular domain, is represented as a horizontal blue line. Error bars represent the standard deviation of at least four replicates. See also Figure S2.

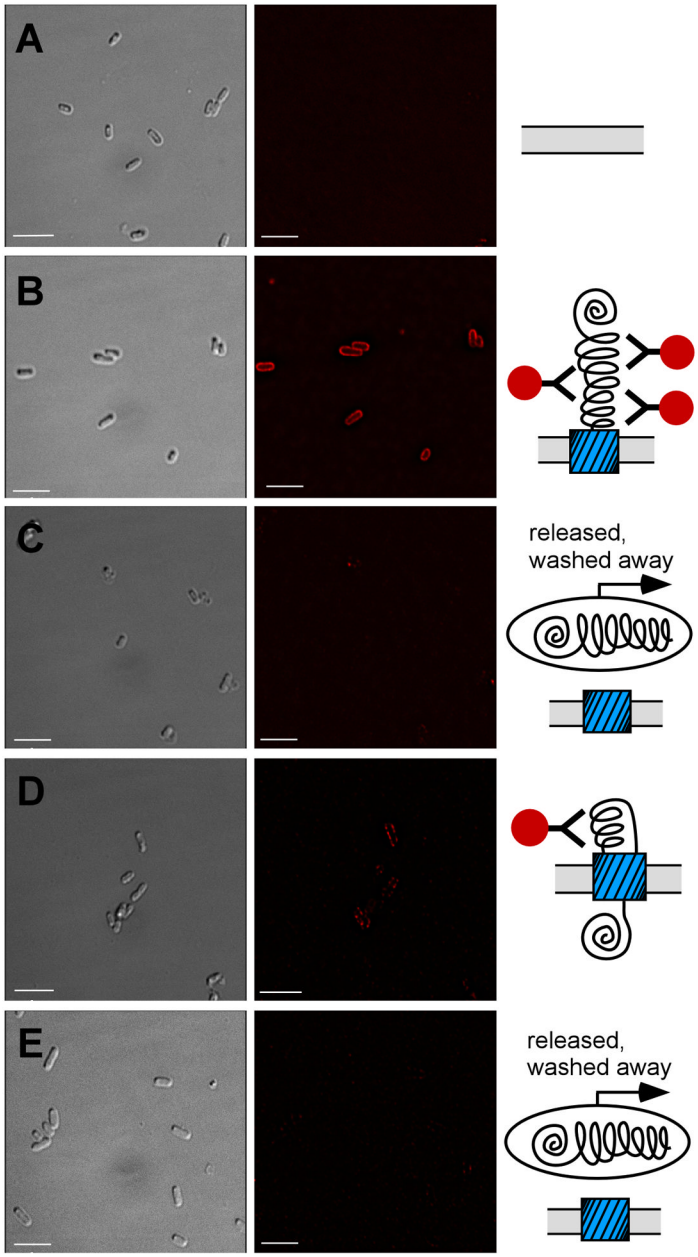

Figure 4.

N-terminally stabilized DHFR-Petβ-helix accumulates at the *E. coli* cell surface. Immunofluorescence microscopy images of *E. coli* expressing (**A**) empty vector, (**B**) an uncleavable PetΔprotease mutant (N1018G/N1019I) that acts as a positive control for surface display of the Pet passenger (Navarro-Garcia et al., 2001) and preserves Pet epitopes recognized by the anti-Pet passenger domain polyclonal antibody in the DHFR chimera constructs, (**C)** DHFR-Petβ-helix, (**D**) more stable DHFR-Petβ-helix D27N, or (**E**) less stable DHFR-Petβ-helix I155A. Left panel, bright field images of *E. coli* expressing each construct. Right panel, corresponding Cy3 fluorescence images of the same field. Scale bar corresponds to 5 μm.

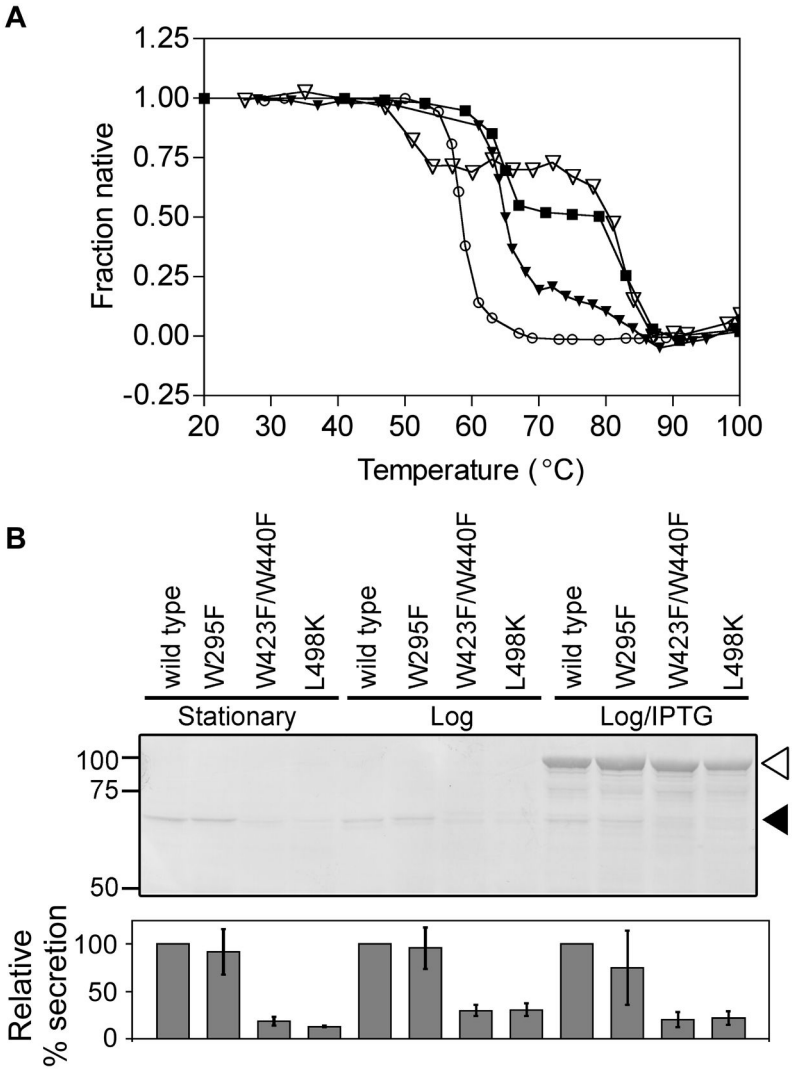

Figure 5.

Decreasing pertactin C-terminal passenger stability, but not N-terminal stability, reduces OM secretion. (**A**) Thermal unfolding of purified wild type pertactin passenger (filled squares), N-terminal mutant W295F (open triangles), C-terminal single mutant L498K (filled triangles), and the globally-destabilizing C-terminal double mutant W423F/W446F (open circles). (**B**) OM secretion of wild type and mutant pertactin passengers. *E. coli* whole cell lysates were separated by SDS-PAGE and detected using an anti-pertactin polyclonal antibody. Relative percentages of processed pertactin passenger (filled arrowhead) were quantified and normalized to wild type in each growth condition. Error bars represent the standard deviation of three to six independent trials. Open arrowhead: unprocessed pre-protein (passenger+β-domain).

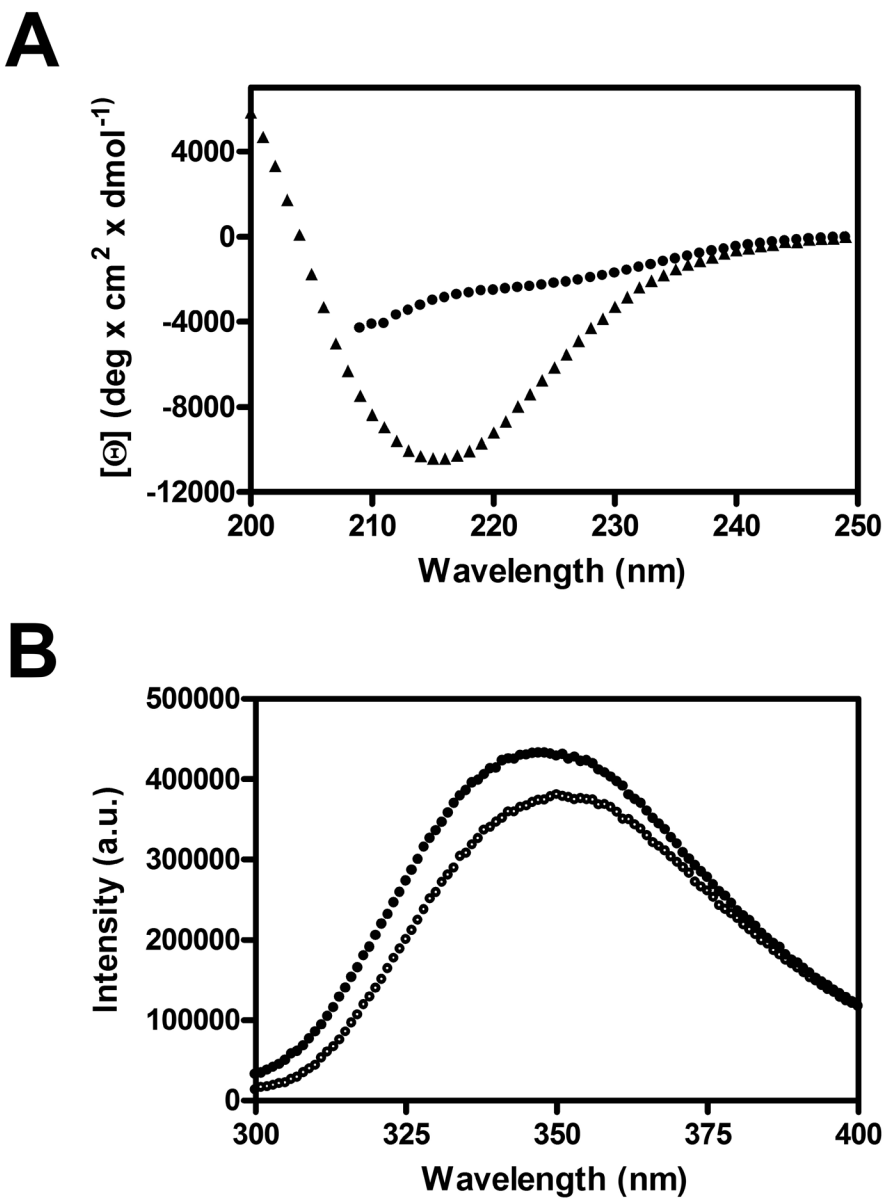

Figure 6.

The N-terminus of the pertactin passenger does not adopt regular structure. (**A**) Far-UV CD spectra of the entire pertactin passenger domain (*triangles*) and the N-terminal segment (residues 1–334) of the passenger domain (*circles*). The passenger domain spectrum has a minimum around 218 nm as well as a positive signal around 200 nm, typical for β-sheet structure, while the N-terminal segment shows no significant contribution of α-helical or β-sheet structure. (**B**) Fluorescence spectra of the N-terminal segment under folding (0 M GdnHCl) and unfolding (6 M GdnHCl) conditions. The lack of significant changes for the maximum emission wavelength or total fluorescence intensity imply no significant structural changes in the protein upon addition of GdnHCl.

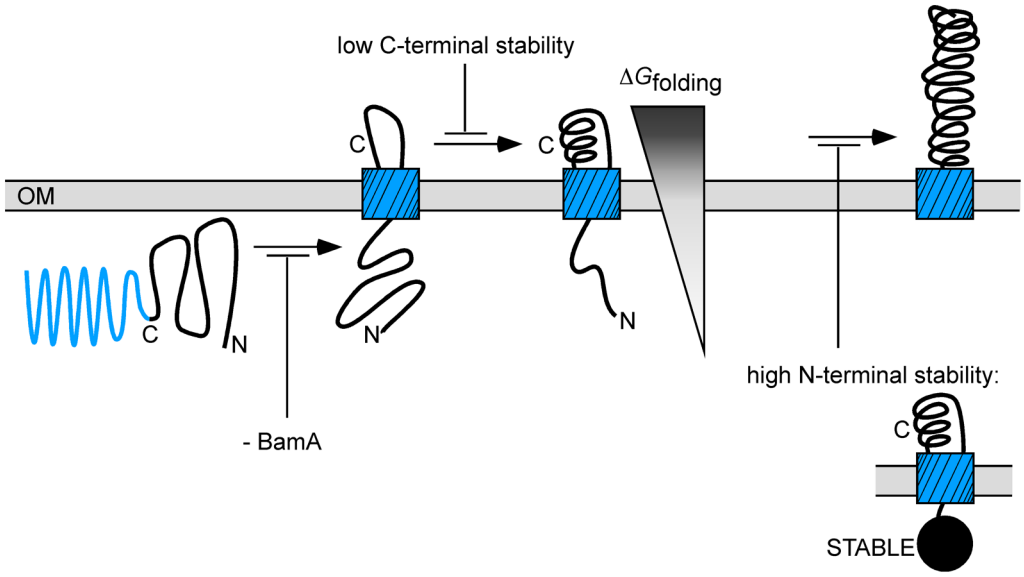

Figure 7.

Model for outer membrane (OM) secretion of an autotransporter (AT) passenger domain. Insertion of the C-terminal AT β-domain porin is facilitated by BamA (Jain and Goldberg, 2007; Ieva and Bernstein, 2009), but it is currently unclear whether BamA is involved in passenger transport across the OM. The C-terminus of the passenger domain crosses the OM first (Junker et al., 2009). *In vitro*, the passenger C-terminus is more stable than the N-terminus (Junker et al., 2006) and here we have shown that reducing passenger domain C-terminal stability reduces OM secretion efficiency. In contrast, destabilizing the passenger N-terminus increases OM secretion efficiency, while stabilizing the N-terminus reduces secretion. These results indicate that localized regions of passenger stability, specifically a C-terminus more stable than the N-terminus, create an anisotropic potential that might serve as an energetic driving force for efficient OM secretion.